Climate Risk Management 27 (2020) 100207

Contents lists available at ScienceDirect

Climate Risk Management

journal homepage: www.elsevier.com/locate/crm

Inundation modelling for Bangladeshi coasts using downscaled and bias-corrected temperature

Md Kamrul Hasan[a,b,*], Lalit Kumar[a], Tharani Gopalakrishnan[a]

[a] School of Environmental and Rural Science, University of New England, Armidale, NSW 2351, Australia
[b] Department of Agricultural Extension and Rural Development, Patuakhali Science and Technology University, Dumki 8602, Patuakhali, Bangladesh

ARTICLE INFO

Keywords:
Sea-level rise
Temperature projection
Semi-empirical methods
Digital elevation model
Global climate models
Quantile mapping

ABSTRACT

Coastal areas in Bangladesh are at severe risk of inundation by sea-level rise (SLR). Effective adaptation plan requires information about extent and level of projected inundation, which is yet to be localized for Bangladeshi coasts. We used downscaled and bias-corrected temperatures from 28 global climate models to predict SLR around Bangladesh. Based on the extended semi-empirical approach to SLR modelling, this study shows that by 2100, temperature will increase by 1.7 °C (RCP4.5) to 4.4 °C (RCP8.5) relative to 1986–2005 (25.89 °C) and corresponding sea-level will rise by 0.77 m (RCP4.5) to 1.15 m (RCP8.5). The sensitivity of SLR to temperature over 1980–2100 is 2.13 to 3.75 mm/year/°C. Consequently, 2098 km^2 of Bangladesh is likely to be inundated under 1 m SLR, affecting the coast and river-banks with potential for significant indirect effects, including increased soil and water salinity and underground water contamination. This study provides modelled projection of SLR and inundation for the 21st century, and thus, it should provide useful information for adaptation planning and SLR preparedness in Bangladesh.

1. Introduction

Bangladesh has well-known deltaic floodplains exposed to the Bay of Bengal under notable sea-level rise (SLR) risk; increased by its flat topography and dynamic deltaic morphology (CCC, 2016). Though global warming is blamed for SLR (Orlić and Pasarić, 2013), the underlying dynamic processes and mechanisms of SLR are too complex to modelize (Horton et al., 2014; Rahmstorf, 2007). Three major processes are thought to influence global SLR, which are melting of glaciers and ice-sheets, thermal expansion of ocean water, and varying water storage on land (Chao et al., 2008; Forsberg et al., 2017; IPCC, 2007b; Moon et al., 2018). This simple explanation tends to overlook many other important geological processes. While macro-scale (10–100 m) paleo-sea-level rise and fall are attributed to marine transgression and regression along with other geologic processes. Contribution of floating- and land-ice on melting to SLR is limited because of several phenomena, such as strong gravity of polar regions, equatorial bulge, polar flattening and lower elevation of spheroidal earth surface in the pole, which act against SLR (Khan, 2019). According to Mörner (2017), thermal expansion of ocean water is always cyclic and restricted to flow towards the coast because of a strong relief of the sea level surface. Furthermore, thermal expansion decreases to zero at the coast where seawater line ends up, and this expansion can contribute not more than 10 cm to SLR by the end of the 21st century. Thus, glacial eustasy and thermal expansion are unable to explain the entire process of SLR without rotational eustasy (e.g., a 60-year cycle), which is linked to planetary influence on the sun, the earth and the

* Corresponding author at: School of Environmental and Rural Science, University of New England, Armidale, NSW 2351, Australia.
E-mail addresses: mhasan7@myune.edu.au, kamrulext@pstu.ac.bd, kamrulext@gmail.com (M.K. Hasan), lkumar@une.edu.au (L. Kumar), tgopalak@myune.edu.au (T. Gopalakrishnan).
URL: http://lalit-kumar.com/ (L. Kumar).

https://doi.org/10.1016/j.crm.2019.100207
Received 10 September 2019; Received in revised form 8 December 2019; Accepted 15 December 2019
Available online 24 December 2019

earth-moon system (Mörner, 2019a,b).

The reasons of SLR have been under research and debate for years (Chao et al., 2008), but SLR along Bangladeshi coast is evident from tide-gauge data (Pethick and Orford, 2013). Even if temperature stabilises by 2100, sea-level stabilisation will take many years, and SLR will represent a continuing long-term threat to low-lying coastal areas (Brown et al., 2018; IPCC, 2018). Projected SLR is a global risk and increases flood impacts (Nicholls, 2004), but has local differentiation (IPCC, 2014). By the 2080 s, SLR could bring a loss of up to 22% coastal wetlands on a global scale that loss could even reach 70% when combined with other losses from human actions (Nicholls et al., 1999). Since 1998 the Germanwatch index (Eckstein et al., 2019) has consistently reported Bangladesh as one of the most vulnerable countries to climate change. Impacts of climate change and SLR in Bangladesh are widely accepted issues, but regional vulnerability is little understood (Auerbach et al., 2015; Unnikrishnan and Shankar, 2007).

Coastal agricultural in Bangladesh is adversely affected by SLR (Ruane et al., 2013). Research in Bangladesh concerning SLR has received greater importance since the IPCC (IPCC, 2007a) presented it as one of the most vulnerable places. Contemporary literature provides confusing messages; in many cases SLR is presented as a great concern (Ali and Kader, 2015) and sometimes as little (Brammer, 2014) or no concern (Mörner, 2010). Estimations of SLR based on available tide-gauge data have been presented without extrapolations for future periods (Sarwar, 2013). Attempts have been made to predict SLR (Brown et al., 2018), but regional projections using multiple global climate models (GCMs) are absent. Besides, SLR projection is still a challenge (Bittermann et al., 2013), since incorporating ice sheets and glacier dynamics in SLR models is necessary but their poorly understood behaviour (Vermeer and Rahmstorf, 2009) could increase uncertainty in process-based modelling. Therefore, semi-empirical sea-level projection has drawn more extensive attention. While SLR projection requires a large number of predictors, the semi-empirical approach has opened a new window to ease the computation (Vermeer and Rahmstorf, 2009). We used this approach to update the regional projection of SLR for Bangladesh.

For Bangladesh, generalised projections of SLR for 2100 are reported with an upper limit between 0.88 m (MOEF, 2005) and 1.00 m (Agrawala et al., 2003), with conflicting reports on estimated SLR rates (Brammer, 2014; Pethick and Orford, 2013; Singh, 2002; Unnikrishnan and Shankar, 2007). For example, studies have mentioned that only 10% of land area of Bangladesh is above 1 m mean sea level (Karim and Mimura, 2008) and 28% of population is under the threat of SLR (Ali and Kader, 2015). Potential inundation has been presented as 11% (CCC, 2016), 13% (Nishat and Mukherjee, 2013) and 17.5% of coastal areas (Sarwar and Khan, 2007) due to a SLR of 0.45, 0.62 and 1.00 m, respectively. None of the previous studies used downscaled and bias-corrected GCM data and appropriate digital elevation models (DEM) to model SLR in Bangladesh, which is necessary for adaptation planning. The divergence in the existing SLR literature is mainly due to a lack of using an ensemble of GCMs, bias-corrected data and quality DEM for inundation mapping, and partly due to excluding embankments that act as man-made resilience against SLR (Auerbach et al., 2015; Brammer, 2014; Inman, 2009). LiDAR-based DEM is yet to be produced for Bangladesh. Although DEM from Advance Land Observing Satellite (ALOS) is freely available to the public (JAXA, 2019), it has not been applied for coastal inundation mapping for Bangladesh. The ALOS DEM is the most accurate freely available global surface model (Alganci et al., 2018; Florinsky et al., 2018). To bridge this gap we used a semi-empirical method (Vermeer and Rahmstorf, 2009), ALOS DEM, temperature data from 29 weather stations and an ensemble of 28 downscaled and bias-corrected GCMs to model SLR and more accurately quantify the future extent of inundation in the coastal areas of Bangladesh.

2. Material and methods

This paper focused on the projection of sea-level rise (SLR) for the 21st century in the coastal areas exposed to the Bay of Bengal. As we have used semi-empirical method to project SLR, we needed to project temperature for the same period. A total of 28 GCMs (Appendix Table A.1) data from Coupled Model Intercomparison Project phase 5 (CMIP5) were used to downscale the temperature data for 29 weather stations (Appendix Figure A.1) in Bangladesh. After projection of SLR using downscaled temperature, we prepared an inundation mapping using ALOS AW3D30 DSM (JAXA, 2019). Finally, we calculated inundation area of one meter SLR. To understand the potentially affected areas and population, we plotted area and population data across different levels of elevation. Statistical analysis and visualisation were done by RStudio (Version 1.1.383) and spatial analysis and cartography were performed by ArcGIS for Desktop (Version 10.4.1.5686).

Daily minimum and maximum average near-surface air temperature data of 28 GCM models of CMIP5 under RCP4.5 and RCP8.5 were downloaded from https://esgf-node.llnl.gov/projects/cmip5/. We excluded the RCP2.6 and RCP6.0 because RCP2.6 scenario is challenging to achieve and RCP 6.0 is already in between the RCP4.5 (lower emission) and RCP8.5 (higher emission) (Moss et al., 2010; Wang and Chen, 2014). We obtained minimum and maximum temperature data of 29 weather stations from Bangladesh Meteorological Department. We used rSQM::DailyExtractAll() (Cho et al., 2018) R function for downscaling the model data to geographical locations of the weather stations. We averaged the minimum and maximum temperature from the downscaled series to obtain a temperature series for each of the RCPs and historical period. Missing data in the observed temperature were imputed using seasonally split missing value imputation technique with na.seasplit() (Moritz et al., 2015) R function. Bias correction of the downscaled data was made using traditional (Eq. 1) (Gudmundsson et al., 2012; Wang and Chen, 2014) and improved (Eq. 2) (Li et al., 2010; Wang and Chen, 2014) quantile mapping. Improved method is superior in the sense that it considers the difference between the data distributions for the reference and the projected periods for a model whereas traditional quantile mapping assumes similar distributions for both the periods (Wang and Chen, 2014).

$$\tilde{x}_{traditional} = F_{o\text{-}c}^{-1} \cdot F_{m\text{-}c}(x_m) = h_1(x_m) \quad (1)$$

$$\tilde{x}_{improved} = x_m + F_{o\text{-}c}^{-1} \cdot F_{m\text{-}p}(x_m) - F_{m\text{-}c}^{-1} \cdot F_{m\text{-}p}(x_m) = x_m + h_2(x_m) - h_3(x_m) \quad (2)$$

where $\tilde{x}_{traditional}$ and $\tilde{x}_{improved}$ are bias-corrected outputs, x_m is downscaled model outputs (RCP4.5 and RCP8.5) either in the reference or projection period, $F_{o\text{-}c}^{-1}$ is quantile function of observed data in the reference period, $F_{m\text{-}c}^{-1}$ quantile function of model output in the reference period, $F_{m\text{-}c}$ cumulative distribution function (CDF) of model output in the reference period, $F_{m\text{-}p}$ CDF of model outputs in the projection period and h_1, h_2 and h_3 represent transfer functions. Transfer function, h_1 for example, was computed in two steps (Wang and Chen, 2014): (i) sorting both the observed and model time series for the reference period in ascending order of values and preparing a quantile-quantile plot; and (ii) applying cubic smoothing splines to fit the quantile-quantile plot to find the h_1 using qmap::fitQmapSSPLIN() (Gudmundsson et al., 2012) R function. Finally, h_1 was used with model outputs to obtain the bias-corrected outputs with the help of qmap::doQmapSSPLIN() (Gudmundsson et al., 2012) R function.

Depending on the x_m, six bias-corrected outputs were obtained: (i) historical traditional (1988–2007); (ii) historical improved (1988–2007); (iii) projected traditional (2008–2100) under RCP4.5; (iv) projected improved (2008–2100) under RCP4.5; (v) projected traditional (2008–2100) under RCP8.5; and (vi) projected improved (2008–2100) under RCP8.5. We set calibration period to 1988–2007 that was used for bias correction, validation to 2008–2017 that was used to verify the bias-corrected outputs and projection to 2018–2100. Daily temperature series were annualised by using yearly means. Bias-corrected and predicted temperature data were plotted over the observed data for the calibration and validation periods (Appendix Figure A.3 and Figure A.4) to test the bias correction accuracy.

The sea level was projected using tide gauge data of stations located in Bangladesh (Appendix Figure A.5) downloaded from UHSLC dataset (Caldwell et al., 2015) supplied by Bangladesh Inland Water Transport Authority. We could not use data of all the seven stations because of a lot of missing values and inconsistent temporal span of data. We selected Hiron Point and Char Changa stations considering the maximum time span and completeness of time series from 1980 to 2000. We imputed missing values with na.seasplit() (Moritz et al., 2015) R function that takes into account the seasonal variation present in the time series. Finally, we averaged the daily time series of sea levels of Hiron Point and Char Changa to make a yearly time series of the observed SLR.

We extracted the temperature trends from the yearly series to feed into the SLR modelling. Singular spectrum analysis (SSA) was done to separate the trends and remove the seasonality and random noise components of the series. The SSA is a well-developed trend extraction statistical technique used in time series analysis and forecasting (Golyandina and Korobeynikov, 2014). The 'Rssa' R package was used for SSA-smoothing of the time series with low pass filters (Golyandina and Korobeynikov, 2014; Golyandina et al., 2015; Korobeynikov, 2010). A 15-year window length was used for temperatures of 1980–2100 period and a length of 10-year was used for observed temperature and sea-level data of 1980–2000. To find out the trends in the reconstructed series, we determined eigentriple grouping parameters with the help of scree plots of the eigenvalues (Appendix Figure A.6) and weighted-correlation matrices (Appendix Figure A.7) (Golyandina et al., 2018). For all the cases of the time series used in this paper, the first component of the reconstructed series represented the trend because it showed weighted-orthogonality (zero weighted-correlation) with the other components (Golyandina et al., 2001). The extracted SSA-smoothed trends were plotted over the yearly mean values of the respective series to validate the conformity of the trends with the original series (Appendix Figure A.8).

After having all the SSA-smoothed trends, we used an extended version of semi-empirical approaches to SLR modelling which is called dual model that can be expressed as the Eq. (3) (Vermeer and Rahmstorf, 2009).

$$dH/dt = a(T - T_0) + b\, dT/dt \quad (3)$$

where dH/dt is the time series of rate of sea-level change, dT/dt is the time series of rate of temperature change, T is temperature time series, T_0 is the temperature when sea level and temperature are at an equilibrium, a and b are the coefficient to be determined. We estimated a and b using linear regression after calibrating the T_0 to a value that results in zero intercept. We found that T_0 was 25.17 °C, a was 3.805 and b was 26.38. Once a time series of rate of sea-level change was obtained, corresponding sea levels were computed by integrating the equation (3) over a unit time.

After projecting SLR, we examined how much coastal areas could be inundated by 2100. A DEM prepared from ALOS World 3D – 30 m (AW3D30) Version 2.2 © JAXA was used for inundation mapping because LiDAR-based DEM was unavailable. It had one-meter vertical and 30 m spatial resolution (JAXA, 2019) and vertical accuracy of the ALOS DEM has a considerably low root mean square error (1.78 m) (Caglar et al., 2018). Twenty-eight tiles of $1^\circ \times 1^\circ$ size covering entire Bangladesh, downloaded from https://www.eorc.jaxa.jp/ALOS/en/aw3d30/data/index.htm, were mosaiced to a single raster and clipped to the boundary of Bangladesh shapefile. Areas below one-meter elevation were extracted from the DEM and hydrologically connected inundation mapping of one-meter SLR was prepared. An eight-side connectivity rule was followed to map the inundated areas to make it more realistic. Application of the hydrological connectivity rule is an improvement of a simple 'bathtub' approach because this rule will allow a grid cell below the critical elevation to be inundated only if any of the adjacent cells are below that elevation (previously flooded, open water or just lower elevation) started from the seawater (Poulter and Halpin, 2008). Ensuring hydrologic connection to the ocean is one of the best recommended methods for coastal inundation (Gesch, 2018). This study did not examine the interaction of SLR with other dynamic and complex floods during the modelling period, and therefore, we did not use more advanced techniques of inundation modelling, for example, Delft 3D hydrodynamic model as used by Haque et al. (2018) and Adnan et al. (2019). We also showed the proportion of population in different elevations. Population data were obtained from Bangladesh Bureau of Statistics (BBS, 2014) that were merged with a union-level shapefile of Bangladesh. Projected population data of Bangladesh in the 21st century were obtained from population prospects of the United Nations (UN, 2017b).

Accuracy of a model depends on the accuracy and suitability of the data used in the analysis. Considering the availability, we only used 20-year sea-level data that might be too short span for a long-term projection. The SLR is not only triggered by thermal

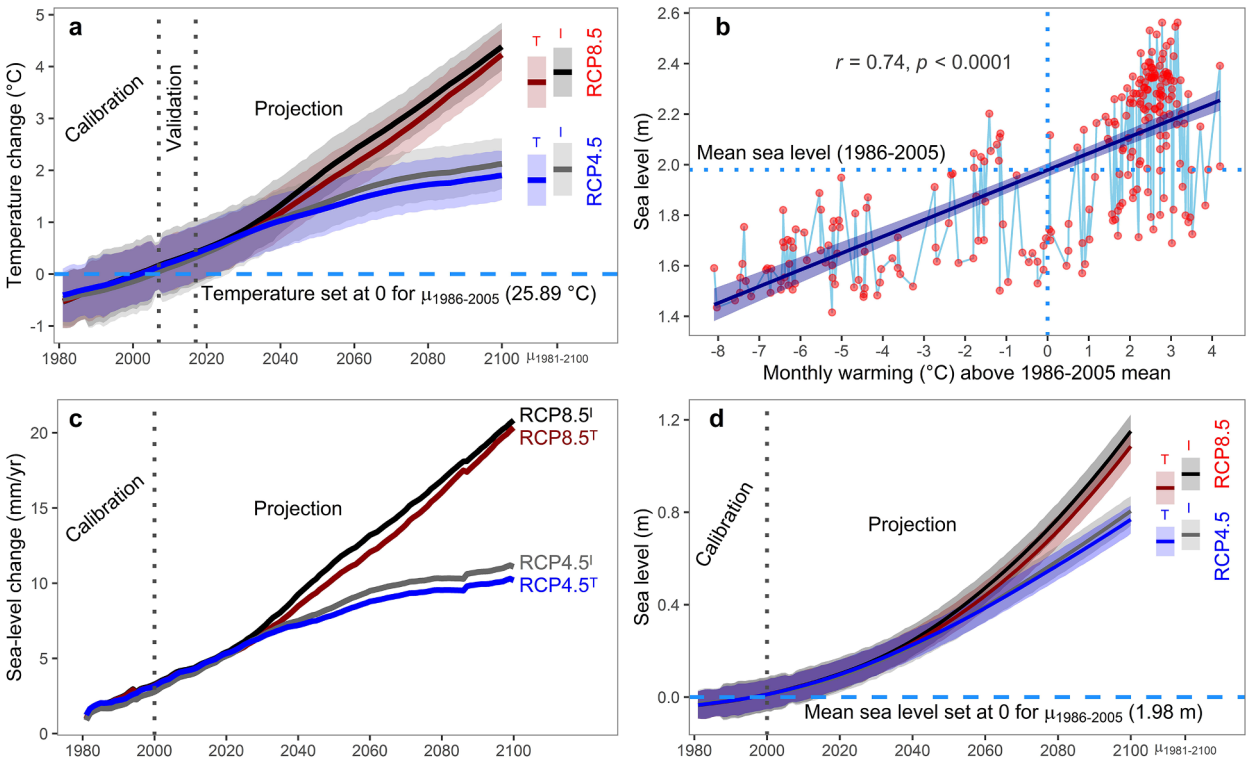

Fig. 1. Semi-empirical sea-level projection. **a**, SSA smoothed series of GCM downscaled and bias-corrected projected temperature using RCP4.5 and RCP8.5 with improved (indicated by ^{I}) and traditional (indicated by ^{T}) techniques. Shaded bands show yearly one standard error of the respective monthly series. Vertical bars represent one standard errors and average trends over 2081–2100. **b**, Scatter plot showing the relationship between monthly temperature and sea level for the period of 1980–2000. Shaded band represent 95% confidence interval of estimated regression line. **c**, Projected rate of sea-level change using different RCPs and projection algorithms. **d**, Projected sea level compared to 1986–2005. Lines show sea level and shaded bands show 95% confidence interval of yearly means of the respective monthly series.

expansion of water that is taken into account by the semi-empirical approach, but it is also influenced by many other factors, such as positively by ice sheet melting and ice formation (Rahmstorf, 2007) and negatively by water impoundment in artificial reservoirs (Chao et al., 2008) and land subsidence (Hanebuth et al., 2013). Besides, marine transgression, regression, and glacial-, tectonic- and rotational-eustasy play a major role in the distribution of ocean water mass (Khan, 2019; Mörner, 2019a). Therefore, the sea level has never been an isolated physical phenomenon. The factors influencing SLR are variable, and non-linearly and unpredictably dynamic, making them difficult to incorporate in a modelling algorithm where semi-empirical model performs better (Rahmstorf, 2007). We assumed that the semi-empirical-projection model based on historical observations partially accounts for the variations caused by these factors.

3. Results

3.1. Projected temperature and sea level

Projection of temperature was made based on historical data of 29 weather stations across Bangladesh (Appendix Figure A.1) and 28 GCMs (Appendix Table A.1). Fig. 1a, in the case of traditional quantile mapping, shows that by 2100 average temperature will increase by 1.7 °C (RCP4.5) to 4.4 °C (RCP8.5) compared to 1986–2005 (25.89 °C). Bias correction using improved quantile mapping overestimates this increase by 0.1 °C (RCP8.5) to 0.2 °C (RCP4.5). The estimated rate of increase of temperature in Bangladesh for the period of 1980 to 2100 is 0.15 °C to 0.37 °C per decade under RCP4.5 and RCP8.5, respectively.

Monthly temperature and sea level for the period 1980–2000 show a significant positive relationship (Fig. 1b) that was deemed to be sufficient to model temperature-based sea-level projection using semi-empirical approach (Vermeer and Rahmstorf, 2009). Yearly sea-level change rate sharply increased under RCP8.5, but in the case of RCP4.5, it tapers off after 2070 to a reasonably level-off state by the end of the 21st century (Fig. 1c). This yearly sea-level change rate indicates a change in mean sea level compared to the previous consecutive years. It can be as high as 21 mm/year by 2100 (RCP8.5 based on the projected temperature using improved quantile mapping) while it was less than 1.5 mm/year in 1980. The rate of sea-level change was transformed into the mean sea level (Fig. 1d) by integrating the rate of sea-level change over the previous years. The model used in this study suggests that by the end of the 21st century, compared to 1986–2005, mean sea level will increase by 0.77 m (95% confidence [0.71 m, 0.83 m]) to 1.15 m (95%

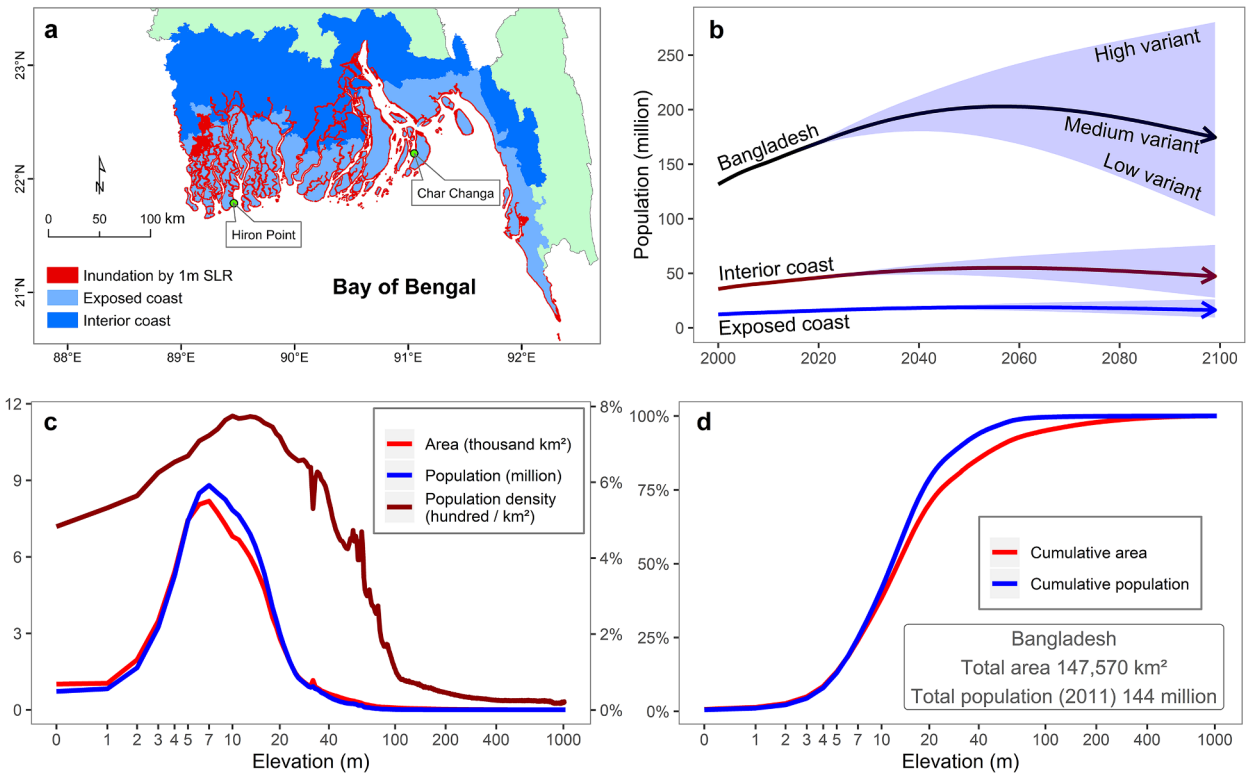

Fig. 2. Estimated inundation and population. **a**, Coastal areas inundated with one-meter SLR above 2014 mean sea level. Locations of the tide gauge stations (Hiron Point and Char Changa) are pointed by the callouts. **b**, Population change in coastal areas and Bangladesh (UN, 2017b). **c**, Population and area for different elevations. **d**, Cumulative population and area for different altitudes. **c-d**, X-axis is log-transformed for gradual stretching of lower elevations.

confidence [1.08 m, 1.22 m]) depending on the RCPs and bias correction methods used for temperature downscaling. Mean SLR by 2050 was projected to be 0.30 m to 0.35 m which is 30 to 39% of the estimated SLR by the end of this century. Yearly average rate of sea-level increase is 6.69 mm (RCP4.5) to 9.88 mm (RCP8.5) for the period of 1980–2100. Even while the temperature trend under RCP4.5 tends to be slower after 2070 (Fig. 1a), the sea level shows continuing upward trend (Fig. 1d) though at a decreased rate (Fig. 1c). The gross relationship between temperature and sea-level rise over 1980–2100 is 2.13 to 3.75 mm/year/°C depending on the RCPs and quantile methods used for bias correction of GCM temperature data.

3.2. Projected inundation and population

In the present sea-level modelling along the coast of Bangladesh, extreme sea-level rise (under RCP8.5, improved quantile mapping) is expected to be 1.15 m by 2100 compared to 1986–2005. However, the DEM for this study was prepared based on the ALOS satellite data captured in 2014 when the average sea level was 0.07 m higher than 1986–2005 (1.98 m). Therefore, inundation mapping was performed based on the one-meter SLR (Fig. 2a), which shows that a narrow strip in the coastal region and riverbanks will be inundated with the increased sea level. According to the model, total area inundated will account for 2,098 km^2 (1.5%) of Bangladesh.

The coastal region was the study area for the inundation mapping. Three criteria, namely mean tidal range, salinity and cyclone risk, are considered to divide the coastal zone into exposed and interior zones (c.f. Fig. 2a). Out of sixty-four districts nine are considered as the coastal zone which can be exposed zone (adjacent to the Bay of Bengal) if the districts demonstrate all the three criteria, otherwise they are termed as interior zone (Islam, 2004; Karim and Mimura, 2008). The inundation area will partly extend beyond the exposed coast (CCC, 2016) and mostly outside the polder and river embankments those were built along the coasts and river banks to prevent tidal surges (Haque et al., 2018). Inundation model shows that the South-west part (Shyamnagar, Kaliganj and Assasuni subdistrict of Satkhira district) of the coastal area will have two larger clusters of inundated areas.

The interior (including the exposed part) and exposed coastal areas (CCC, 2016) share 29% (42,617 km^2) and 13% (18,818 km^2) of total area (147,570 km^2) of Bangladesh, respectively. Total population of Bangladesh was 144 million in 2011 (BBS, 2014) of which 13.4 million (9.3%) and 39.1 million (27.1%) live in the exposed and total coastal areas, respectively. Population dynamics (Fig. 2b) shows that Bangladesh is expected to reach a population maximum of 203 million (172 million low to 239 million high variant) by 2057 followed by a gradual decrease to 174 million by the end of this century, similar to what will be in 2022–2023 (UN,

2017b). Assuming a constant fractional distribution of population in coastal and hinterland, more than one-quarter of the population will be staying in the coastal parts of the country.

Digital elevation model constructed by ALOS surface model (JAXA, 2019) gives an average elevation of 29 m with a high level of variation (*SD* = 60 m, *CV* = 207%, *Median* = 13 m, *Mode* = 7 m) implying a highly positively skewed distribution (Fig. 2c). Population distribution almost perfectly ($r = 0.997$, $p < 0.0001$) follows this pattern of distribution of the area against elevation. Higher population density (> 800 km^{-2}) exists in the lower elevation (< 40 m) areas. Fig. 2d depicts that 80% of the population lives in an elevation of 20 m or less (68% of total area). When 10 m or less elevation (34% of total area) is considered as coastal zone, 36% population falls in this category which is even higher than the estimated population (27.1%) in the total coastal areas of Bangladesh. Another dimension of coastal definition is 100 km buffer zone (UN, 2017a); this comprises 55% of the total area and has 82.5 million (57%) of population. Analysis which satisfies both the 10 m and 100 km assumptions (Appendix Figure A.2) of the definition of coastal area (UN, 2017a) results in 33% of the total area providing home for 37% of the total population of Bangladesh.

4. Discussion

This study modelled SLR along Bangladeshi coasts based on downscaled and bias-corrected temperature for the 21st century. Models used in this study revealed a temperature increase of 1.7 °C (RCP4.5) to 4.4 °C (RCP8.5) and corresponding SLR of 0.77 to 1.15 m by 2100 compared to 1986–2005 (25.89 °C), which is consistent with the country profiles of Bangladesh prepared by the United Nations Development Program (Karmalkar et al., 2010) in 2010 that reported the temperature increase of 1.3 °C (B1 ≈ RCP4.5) to 4.1 °C (A2 ≈ RCP8.5) by 2090s compared to 1970–1999 (24.4 °C). Underestimation of this existing projection was due to using different time periods and emission scenario specifications where the A2 scenario has a lower temperature increase than in RCP8.5 (Rogelj et al., 2012). The IPCC estimated the rise of global temperature by 2081–2100 relative to 1986–2005 as 1.8 °C (RCP4.5) to 3.7 °C (RCP8.5) (IPCC, 2014). For the same time period, we found the increase of temperature as 1.8 °C (RCP4.5) to 3.9 °C (RCP8.5), which implies that if no mitigation measures are taken to limit the greenhouse gas emissions the regional trend of temperature increase in Bangladesh will be higher than the global average increase by 0.2 °C (RCP8.5). Contemporary literature concerning the SLR for Bangladesh presents a wide range of values, for example, 1.3 mm/year (Brammer, 2014; Unnikrishnan and Shankar, 2007), 4.0 mm/year (IPCC, 2014), 7.8 mm/year (Singh, 2002) and 2.8 to 8.8 mm/year (Pethick and Orford, 2013). Over a 100-year period, this range of the SLRs can produce a large uncertainty (0.75 m) in the sea-level projection. Over 1980–2100, model projected averages ($\pm$ standard errors) of SLR were 6.69 ± 0.25 mm/year (RCP4.5, traditional quantile mapping) to 9.88 ± 0.54 mm/year (RCP8.5, improved quantile mapping), which is temporally variable (c.f. Fig. 1c). These findings are more alarming than some other studies, for example, Brammer (2014), IPCC (2014) and Mörner (2010).

In the case of SLR, the IPCC (IPCC, 2014) projected the global mean SLR of 0.64 m (0.45 to 0.82 m) under RCP8.5 (which is 0.96 m in our estimation) by 2081–2100 compared to 1986–2005. Semi-empirical projection in this study has found the increase in sea-level in 2100 as 0.77 m (RCP4.5) to 1.15 m (RCP8.5) compared to 1986–2005. This projection is consistent with the existing reports of SLR between 0.88 m and 1.00 m (Agrawala et al., 2003; MOEF, 2005), however it is based on the bias-corrected data of multiple GCMs to provide a higher level of accuracy and confidence. Finally, the predicted inundated area by the end of 2100 for a one-meter SLR is 11% of the exposed coastal area, 4.9% of the total coastal area and 1.4% of total area of Bangladesh. Previous studies (Sarwar and Khan, 2007) mentioned such inundation as 17.5% of the coastal area of Bangladesh, which is an overestimation compared to our model outputs.

The inundation modelling outputs in this study were influenced by the extensive coastal embankments and polders. Polders are low-lying land enclosed by a raised bund (embankment) that prevents seawater or other flood water entering inside the polder basins. Polder embankments can be breached by water-thrust and local people or overtopped by extreme fluvial floods (Haque and Nicholls, 2018; Rahman and Rahman, 2015). In such cases, polder basins and outsides become hydrologically connected, and an overestimation of inundated area can take place. Similarly, an underestimation can also happen if inundation mapping is done with satellite imageries taken in earlier years and the upgradation of polders is done before the mapping. Inundation model shows that one meter SLR by the end of the 21st century can inundate the coasts and river banks outside the embankments in Bangladesh. Low lying (< 1 m) areas inside the levees were excluded from the inundation mapping because they are hydrologically disconnected by the bunds (polders). The extent of modelled inundation was neither confined only to the exposed coastal zone nor exceeded the interior coastal zone. As most of the inundated areas would be outside the polder embankments, settlements inside the polders would experience direct impacts of SLR to a lesser extent. However, indirect effects of SLR, for example, salinity intrusion, coastal erosion and groundwater contamination (Nicholls and Cazenave, 2010) would impact a larger population of coastal areas. The projected SLR would be a great concern for the settlements and cyclone shelters located outside the polders. The Asian Development Bank (ADB, 2012) reported that a substantial number of people have been living outside the embankments. Damaged polder embankments could be an additional threat for the polder dwellers because repairment of the breached polders takes time (Auerbach et al., 2015). Due to a lack of exact data, we could not estimate the number of houses that would need to be resettled because of the projected SLR.

The inundation model in this study has resulted in two large clusters of inundated areas in Satkhira of Bangladesh (c.f. Fig. 2a). These areas are well protected by polder embankments of 3–5 m heights. They were not inundated even during a super cyclone Sidr in 2007 (Adnan et al., 2019; Haque et al., 2018). This contradictory modelling outcome could have resulted from model uncertainty, and time difference of DEM preparation and cyclone occurrence. The cyclone Sidr occurred in 2007 and the DEM used in this research was based on the satellite imageries captured in 2014. According to the model, inundation areas could expand to a protected area if

polder embankments have been breached, or vertical errors of the DEM minimize the embankment elevations. This study used a DEM based on ALOS AW3D30 imageries of 30 m spatial and 1 m vertical resolution. Its vertical error (root mean square error) can range from 1.78 to 4.4 m (Caglar et al., 2018; Tadono et al., 2016). This error might ignore the embankment heights, and inundation water could expand to the protected polders.

The findings of this study are completely based on semi-empirical model, which relies on temperature as an indicator of SLR and produces approximately 2–3 times higher projections than process-based modelling (Orlić and Pasarić, 2013). The process-based models are still lacking the ability to capture the complexity of responsible mechanisms of SLR (Bittermann et al., 2013). Therefore, we modelled SLR and associated inundation mapping based on an established relation between SLR and temperature (Grinsted et al., 2009). Methods followed in this study starting from temperature downscaling and ending in inundation mapping had uncertainties related to data and calculation procedures. Although assumptions and limitations of the methods are well documented in the literature (e.g., Golyandina et al., 2001; JAXA, 2019; Vermeer and Rahmstorf, 2009), the inundation mapping requires an additional explanation. We only mapped inundation areas that were suggested by the modelled SLR under normal-tide conditions. Coastal inundation is influenced by the interaction of pluvial, fluvial, tidal, fluvio-tidal and storm surge floods (Adnan et al., 2019; Haque and Nicholls, 2018). Precipitation related fluvial flood changes slowly, but sudden abruption can be caused by the storm surge flooding which is common in coastal Bangladesh. The mean tidal range is not static across the coast, rather it varies between 3 m and 6 m. Consequences can be disastrous when storm surges occur during high tide periods. The fluvial flood, on the other hand, can be prolonged due to poor drainage caused by increased sea level (Haque and Nicholls, 2018). However, the inundation model of this study did not examine the interaction of the inundated areas with complex forms of floods in Bangladesh as described by Adnan et al. (2019) and Haque and Nicholls (2018). In the course of inundation mapping, no validity assessment was performed due to a lack of observed inundation data for the inundation period.

5. Conclusions

Based on the semi-empirical approach, this study provides the SLR as 0.77 m (RCP4.5) to 1.15 m (RCP8.5) by the end of the 21st century. A narrow strip outside the polder embankments (2098 km^2) is estimated to be inundated under 1 m SLR. Keeping pace with global temperature trends, greater temperature change will take place in Bangladesh after 2050 and so will be the sea-level change. Even if the temperature and the rate of sea-level change stabilize after 2070 under RCP4.5, sea level will keep rising. Although current analysis of sea-level rise is more shocking than some other studies, the projected inundation does not seem to be frightening for coastal settlements inside the polders. At least 29% of the total population live in the coastal areas. Sea-side and river-side of the dykes are mostly uninhabited and, therefore, direct impact of inundation may be lower, but indirect effects (e.g. salinity intrusion, coastal erosion and groundwater contamination) of the SLR are likely to be experienced by a larger population. However, its impact can be devastating in case of embankment breach in coastal areas. As the projected SLR will inundate mostly river banks and coasts outside the protective embankments, maintenance of the embankments should be a key concern for the government. In many places, the dykes are not strong enough to resist tidal surges. Lengthy repair process of the breached embankments allows seawater to damage standing crop and increase soil salinity. Care should be taken to avoid pluvial flooding and waterlogging inside the dykes, so that rainwater can get a chance to drain out to assist reclamation of saline-degraded soils. This study provides the extent of inundation and other information that would help planners and policymakers to prioritize strategies concerning SLR preparedness having important financial and economic implications. Further research is needed to model SLR more accurately by using LiDAR data, incorporating the complex processes of SLR, examining the interaction of projected SLR with different forms of floods and quantifying the number of people to be displaced by the upcoming SLR along the coasts of Bangladesh.

Data availability

The data generated during the study are available through the corresponding author on request. The source data are available at the following locations: the daily temperature data are available in the Bangladesh Meteorological Department < http://bmd.gov.bd/link/wowspace > and monthly data in Bangladesh Agricultural Research Council < http://climate.barcapps.gov.bd/ > , GCM data of CMIP5 in the ESGF data portal < https://esgf-node.llnl.gov/projects/cmip5/ > , tide gauge data in the UHSLC repository < http://uhslc.soest.hawaii.edu/data/?rq#uh136a > , ALOS (AW3D30) Version 2.2 © JAXA in < https://www.eorc.jaxa.jp/ALOS/en/aw3d30/ > , population data in the Bangladesh Bureau of Statistics < http://203.112.218.65:8008/WebTestApplication/userfiles/Image/National%20Reports/Union%20Statistics.pdf > and population prospects in the United Nations website < https://population.un.org/wpp/Download/Standard/Population/ > .

Code availability

We used standard R package codes as mentioned in the methods.

Acknowledgements

We thank Australian Government for providing financial support for this study via Research Training Program Scholarship.

Author contributions

M.K.H. and L.K. designed the research, M.K.H. modelled the sea-level projection, designed figures and wrote the paper, and T.G. contributed to spatial analysis and inundation mapping. L.K. coordinated the study and all authors discussed the results and commented on the manuscript at all stages.

Competing interests

The authors declare no competing interests.

Appendix A

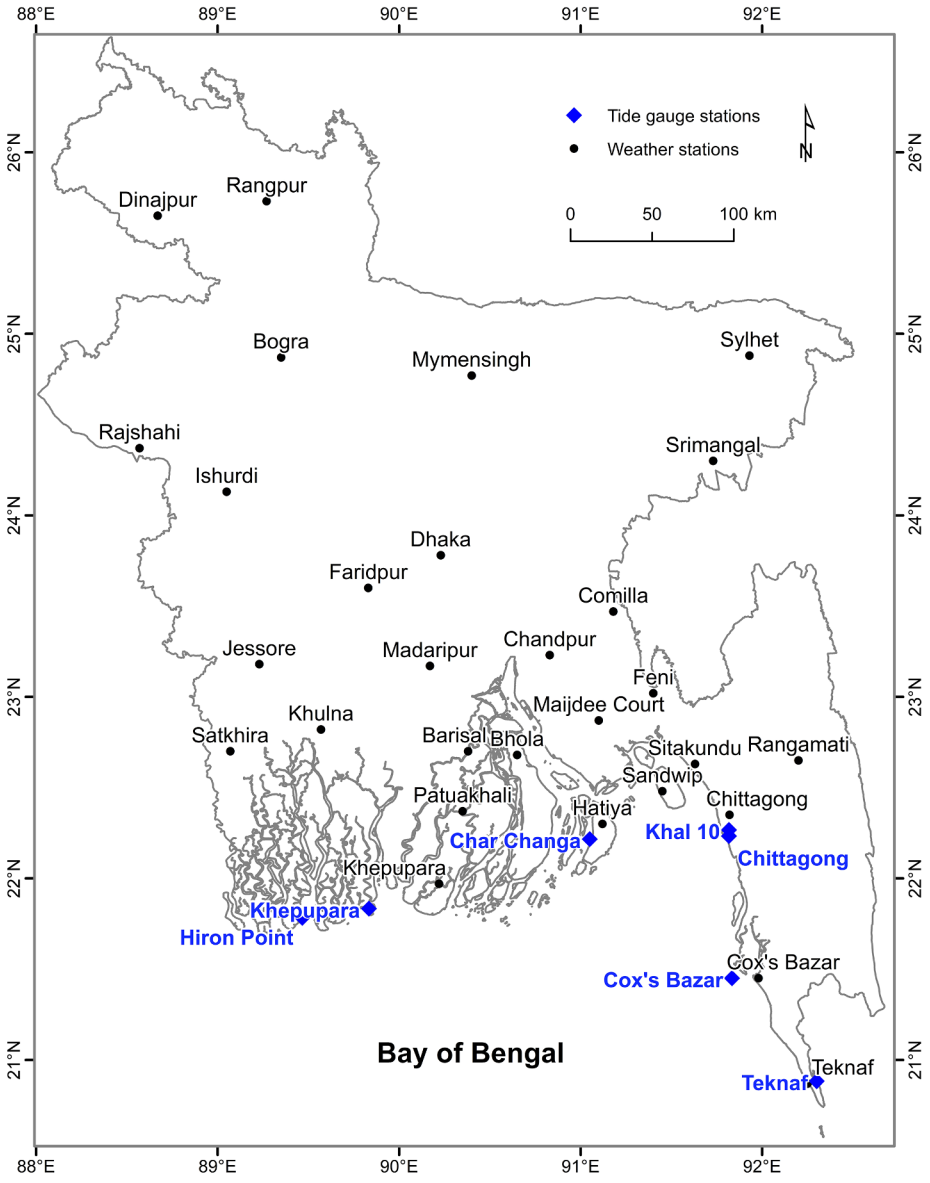

Fig. A.1. Map showing locations of weather and tide gauge stations.

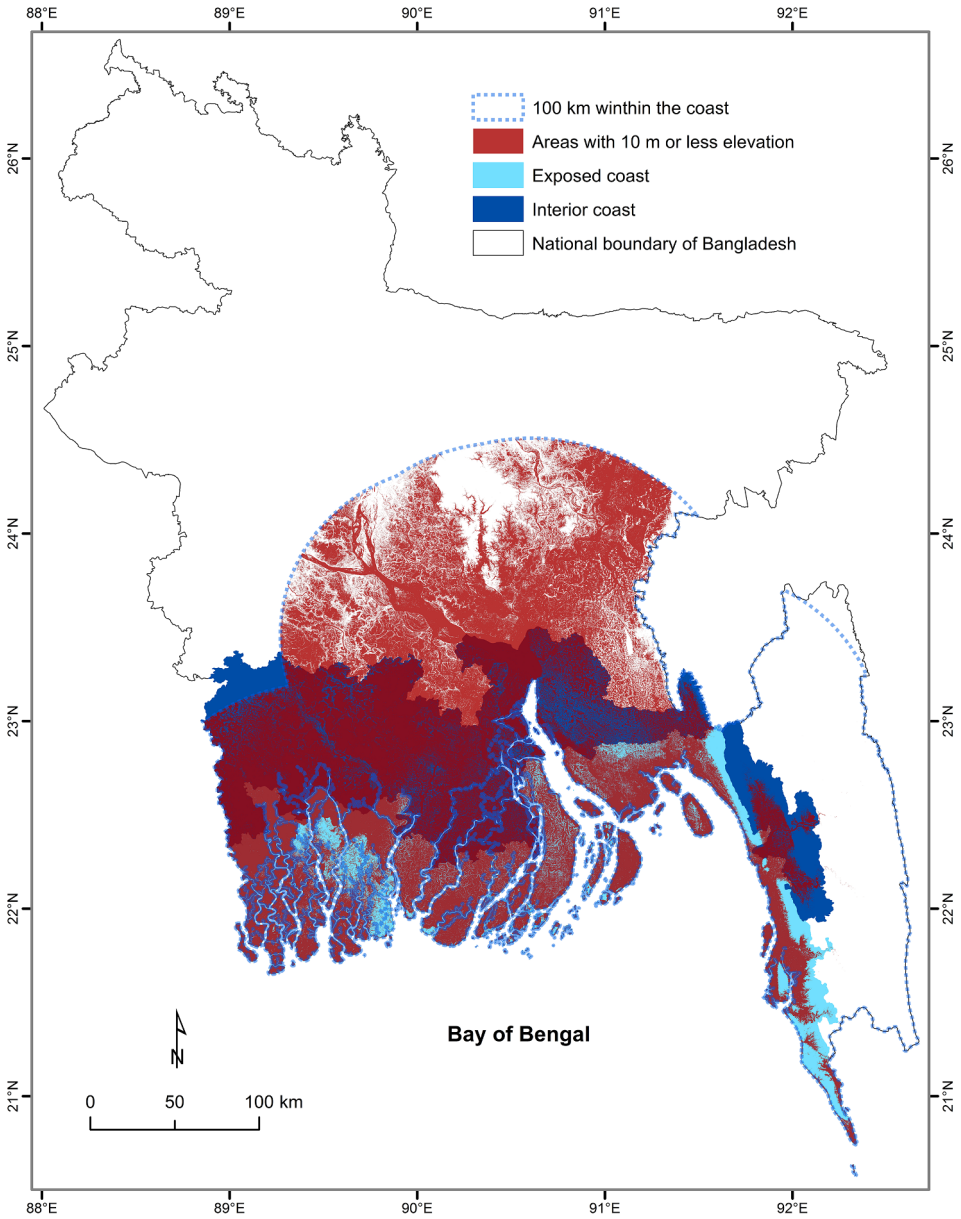

Fig. A.2. Delineation of coastal areas.

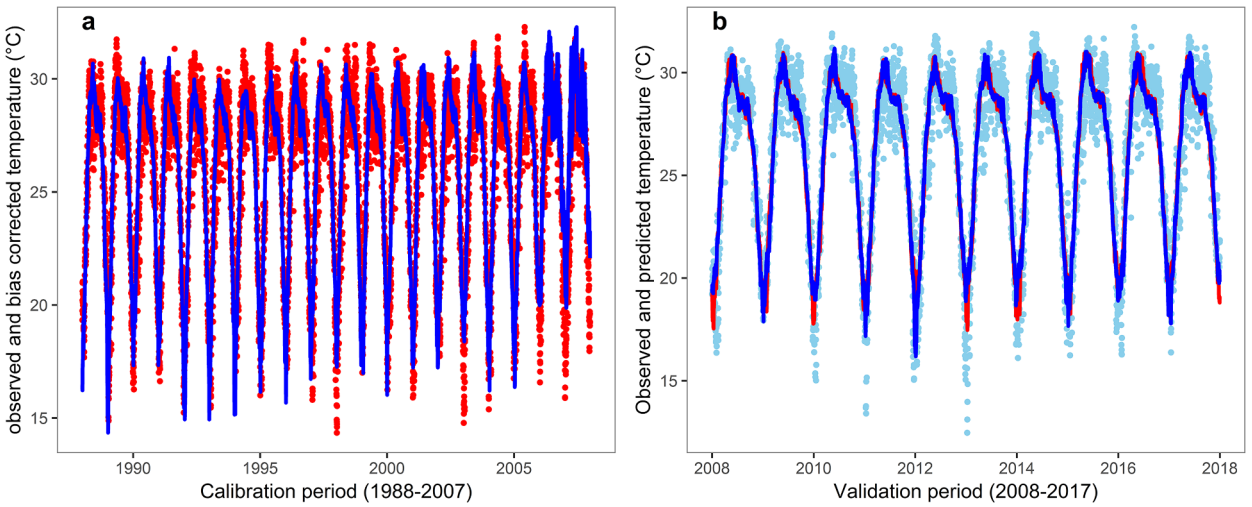

Fig. A.3. Traditional quantile mapping. **a**, Bias corrected temperature (blue) with traditional method and observed temperature (red). Significant correlation ($r = 0.91$, $p < 0.0001$) is found between observed and bias-corrected temperature for the calibration period (1988–2007). **b**, Observed and predicted temperature using traditional method for the validation period (2008–2017). Sky-blue points show observed temperature, blue line shows predicted temperature under RCP 8.5 and red line shows predicted temperature under RCP 4.5. Blue line is almost completely aligned with red line except few lower peaks indicating RCP 8.5 temperature is slightly higher than that of RCP 4.5 even in the validation period. Significant correlation ($r = 0.93$, $p < 0.0001$ for RCP 4.5 and $r = 0.92$, $p < 0.0001$ for RCP 8.5) is found between observed and bias-corrected temperature for the validation period (2008–2017). (For interpretation of the references to colour in this figure legend, the reader is referred to the web version of this article.)

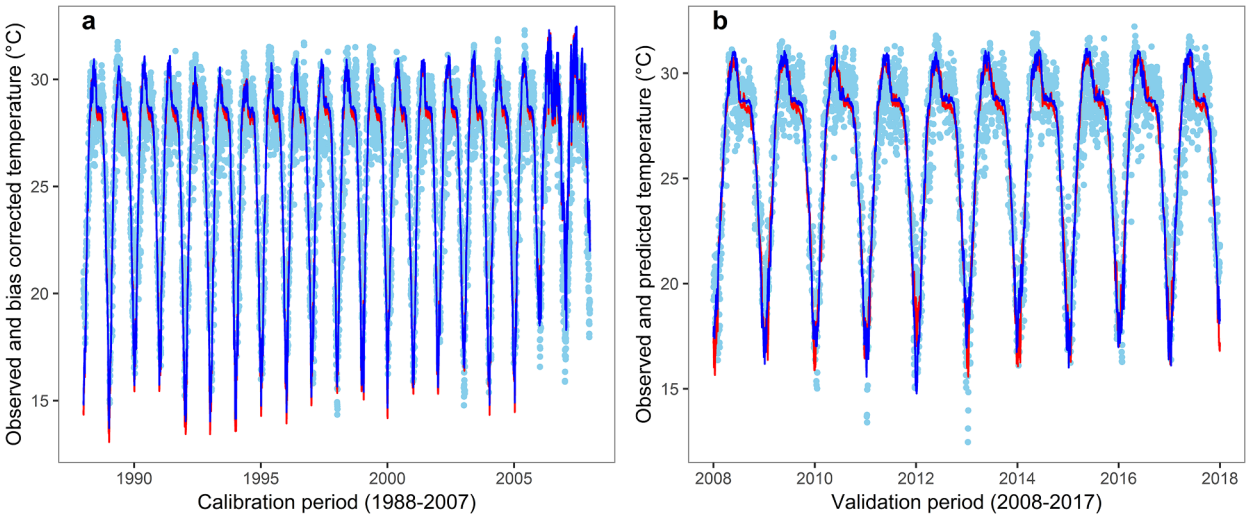

Fig. A.4. Improved quantile mapping. **a**, Bias corrected temperature (blue for RCP 8.5, red for RCP 4.5) with improved method and observed temperature (skyblue). Significant correlation ($r = 0.91$, $p < 0.0001$) is found between observed and bias-corrected temperature for both RCPs for the period of 1988–2007. **b**, Observed and predicted temperature using improved method for the validation period (2008–2017). Sky-blue points show observed temperature, blue line shows predicted temperature under RCP 8.5 and red line shows predicted temperature under RCP 4.5. Blue line is almost completely aligned with red line except few lower peaks indicating RCP 8.5 temperature is slightly higher than that of RCP 4.5. Significant correlation ($r = 0.93$, $p < 0.0001$ for both RCP 4.5 and RCP 8.5) is found between observed and bias-corrected temperature for the validation period (2008–2017). (For interpretation of the references to colour in this figure legend, the reader is referred to the web version of this article.)

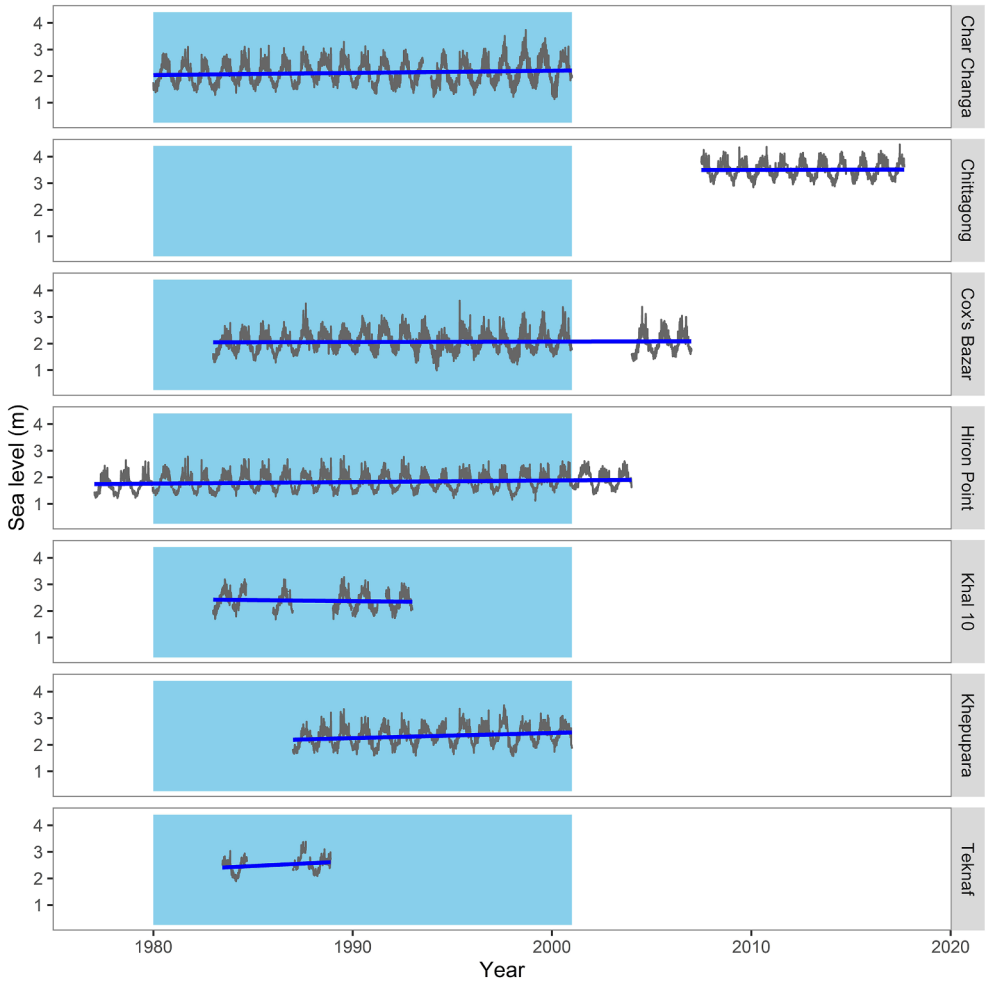

Fig. A.5. Daily timeseries of seven tide gauge stations sea-level data. Shaded areas show temporal windows of 01 January 1980 to 31 December 2000. Blue lines show linear trend of SLR. (For interpretation of the references to colour in this figure legend, the reader is referred to the web version of this article.)

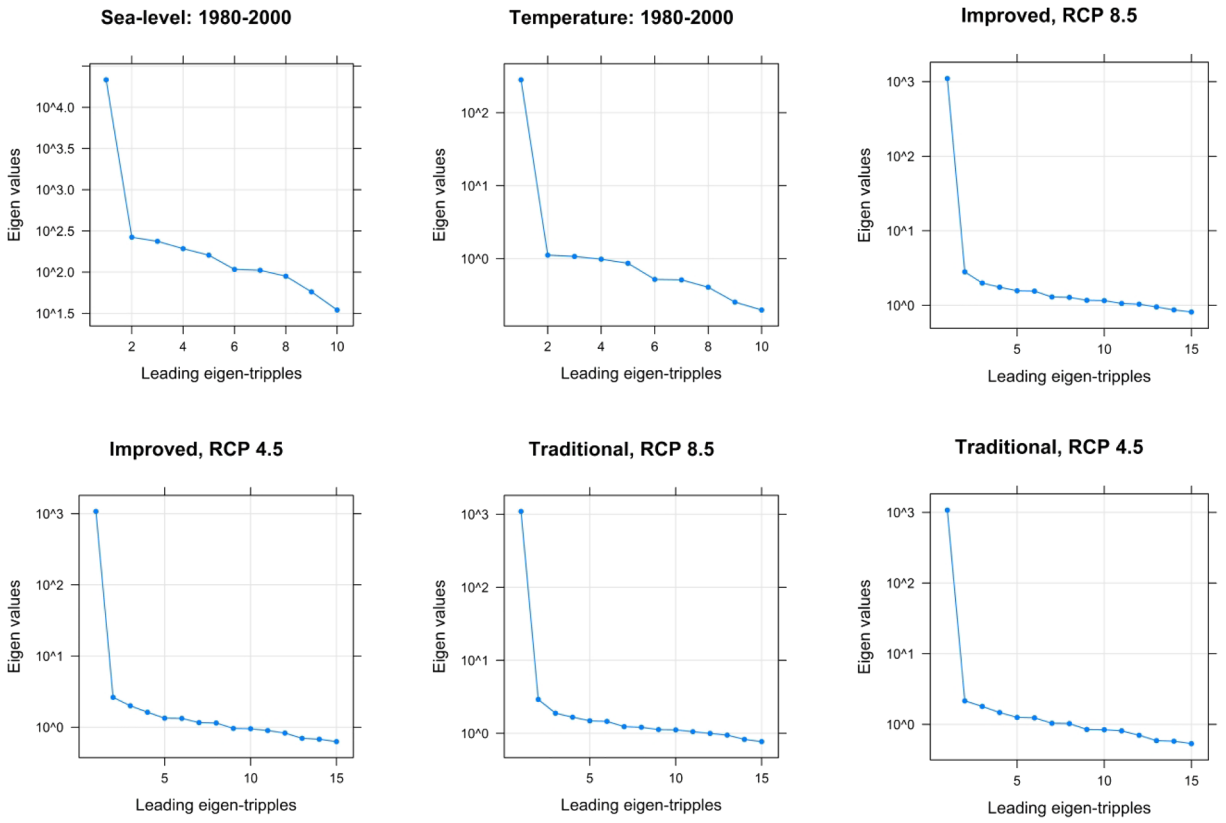

Fig. A.6. Scree plots of different series. In all cases, signal (trend) is contained in the first eigentriple which has the considerably larger eigen values than that of residual components.

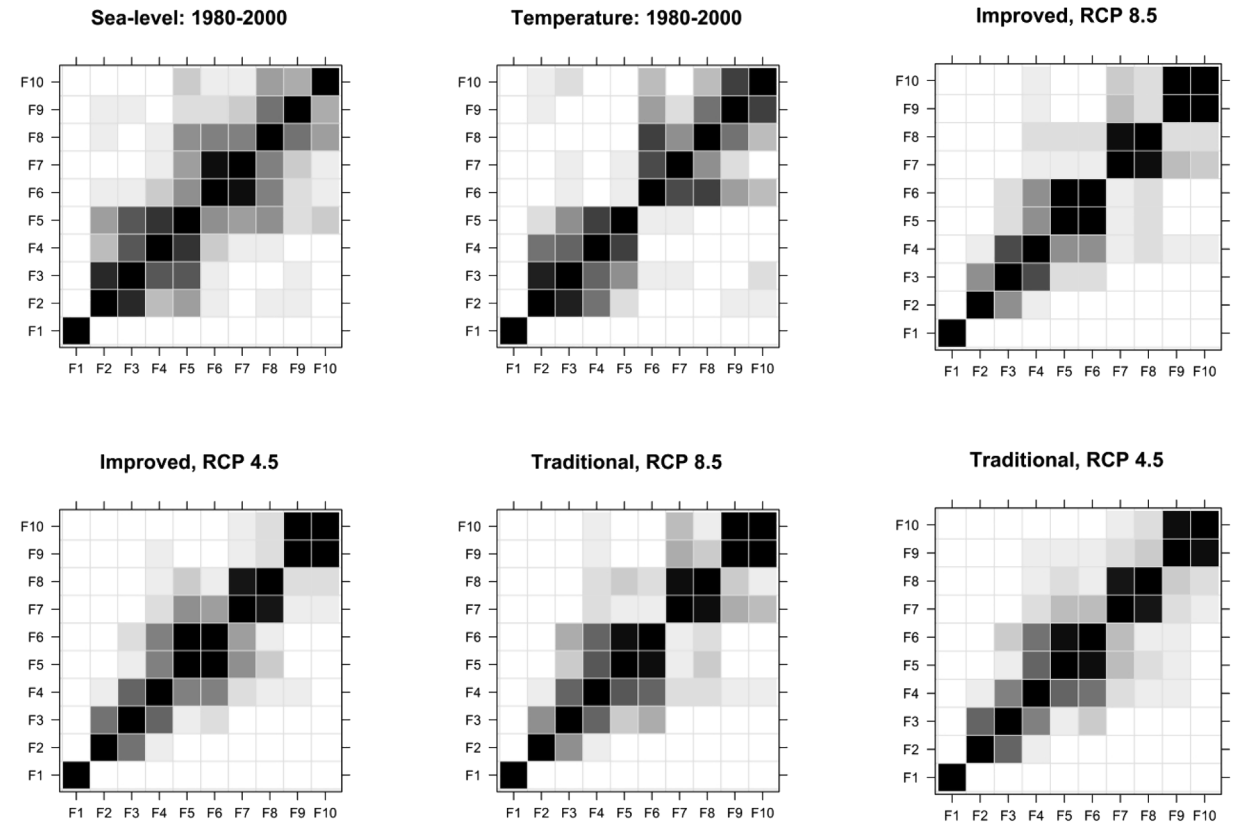

Fig. A.7. W-correlation plots of different series. First component of the eigen vector (F1) represents trend for all the cases because F1 was uncorrelated to other vectors representing seasonality and random errors present in the series. This representativeness of trends is also consistent with the scree plots of the eigen vectors (c.f. Fig. 6).

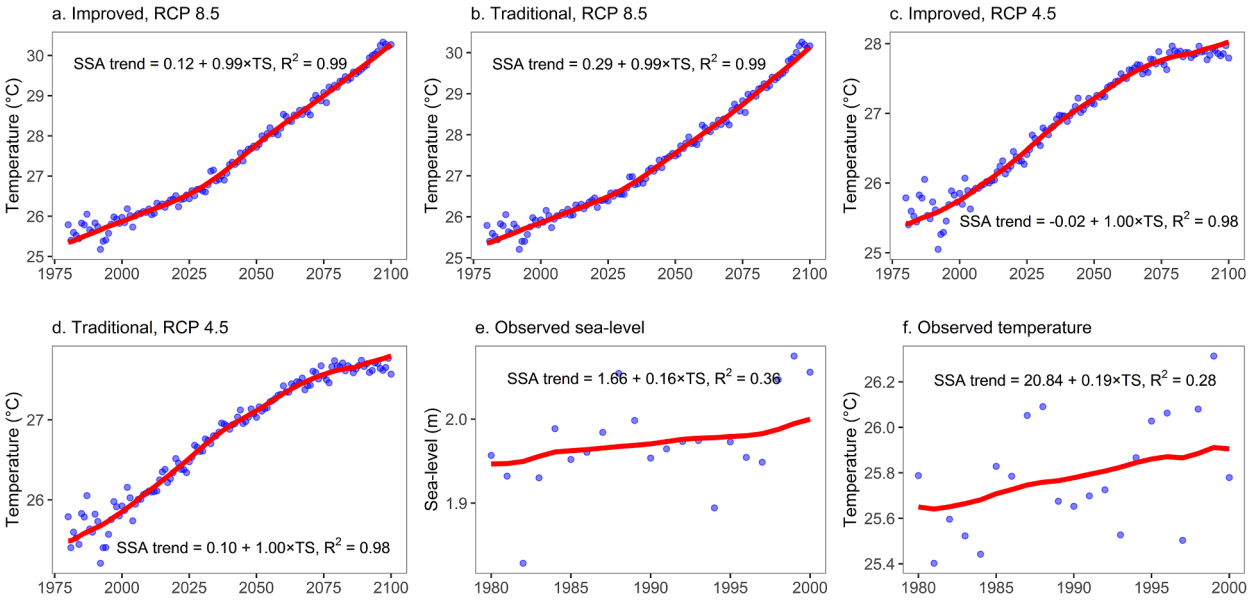

Fig. A.8. SSA-smoothed trends over yearly mean values. **a-f**, SSA-smoothed trends show a good fit on the timeseries (TS) as can be seen from R^2 values.

Table A.1
List of 28 CMIP5 GCM models used for temperature downscaling.

Sl. no.	Model acronym	Modelling center
1	bcc-csm1-1-m	Beijing Climate Center, China Meteorological Administration, china
2	bcc-csm1-1	Beijing Climate Center, China Meteorological Administration, china
3	CanESM2	Canadian Centre for Climate Modelling and Analysis, Canada
4	CCSM4	National Center for Atmospheric Research, USA
5	CESM1-BGC	National Science Foundation - Department of Energy - National Center for Atmospheric Research, USA
6	CESM1-CAM5	National Science Foundation - Department of Energy - National Center for Atmospheric Research, USA
7	CMCC-CM	Centro Euro-Mediterraneo sui Cambiamenti Climatici, Italy
8	CMCC-CMS	Centro Euro-Mediterraneo sui Cambiamenti Climatici, Italy
9	CSIRO-Mk3-6-0	Commonwealth Scientific and Industrial Research Organisation in collaboration with the Queensland Climate Change Centre of Excellence, Australia
10	FGOALS-g2	State Key Laboratory of Numerical Modelling for Atmospheric Sciences and Geophysical Fluid Dynamics, Institute of Atmospheric Physics, Chinese Academy of Sciences and Center for Earth System Science, Tsinghua University, China
11	FGOALS-s2	State Key Laboratory of Numerical Modelling for Atmospheric Sciences and Geophysical Fluid Dynamics, Institute of Atmospheric Physics, Chinese Academy of Sciences; and Center for Earth System Science, Tsinghua University, China
12	GFDL-CM3	National Oceanic and Atmospheric Administration, Geophysical Fluid Dynamics Laboratory, USA
13	GFDL-ESM2G	National Oceanic and Atmospheric Administration, Geophysical Fluid Dynamics Laboratory, USA
14	GFDL-ESM2M	National Oceanic and Atmospheric Administration, Geophysical Fluid Dynamics Laboratory, USA
15	HadGEM2-AO	National Institute of Meteorological Research, Korea Meteorological Administration, Korea
16	HadGEM2-CC	Met Office Hadley Centre (additional HadGEM2-ES realizations contributed by Instituto Nacional de Pesquisas Espaciais), United Kingdom
17	HadGEM2-ES	National Institute of Meteorological Research, Korea Meteorological Administration
18	inmcm4	Institute for Numerical Mathematics, Russia
19	IPSL-CM5A-LR	Institut Pierre-Simon Laplace, France
20	IPSL-CM5A-MR	Institut Pierre-Simon Laplace, France
21	IPSL-CM5B-LR	Institut Pierre-Simon Laplace, France
22	MIROC-ESM-CHEM	Japan Agency for Marine-Earth Science and Technology, Japan
23	MIROC-ESM	Japan Agency for Marine-Earth Science and Technology, Atmosphere and Ocean Research Institute, and National Institute for Environmental Studies, Japan
24	MIROC5	Japan Agency for Marine-Earth Science and Technology, Japan
25	MPI-ESM-LR	Max Planck Institute for Meteorology, Germany
26	MPI-ESM-MR	Max Planck Institute for Nuclear Physics, Germany
27	MRI-CGCM3	Meteorological Research Institute, Japan
28	NorESM1-M	Norwegian Climate Centre, Norway

Appendix B. Supplementary data

Supplementary data to this article can be found online at https://doi.org/10.1016/j.crm.2019.100207.

References

Adnan, M.S.G., Haque, A., Hall, J.W., 2019. Have coastal embankments reduced flooding in Bangladesh? Sci. Total Environ. 682, 405–416.

Agrawala, S., Ota, T., Ahmed, A.U., Smith, J., Van Aalst, M., 2003. Development and Climate Change in Bangladesh: Focus on Coastal Flooding and the Sundarbans. OECD, Paris.

Alganci, U., Besol, B., Sertel, E., 2018. Accuracy assessment of different digital surface models. ISPRS Int. J. Geo-Inf. 7, 114.

Ali, S., Kader, F., 2015. Impact of sea level rise in Bangladesh: a socio-engineering overview. J. Hydrol. Environ. Res. 3, 59–66.

Auerbach, L.W., Goodbred Jr, S.L., Mondal, D.R., Wilson, C.A., Ahmed, K.R., Roy, K., Steckler, M.S., Small, C., Gilligan, J.M., Ackerly, B.A., 2015. Flood risk of natural and embanked landscapes on the Ganges-Brahmaputra tidal delta plain. Nat. Clim. Change 5, 153.

BBS, 2014. Bangladesh Population and Housing Census 2011: Union Statistics. Bangladesh Bureau of Statistics, Ministry of Planning, Bangladesh.

Bittermann, K., Rahmstorf, S., Perrette, M., Vermeer, M., 2013. Predictability of twentieth century sea-level rise from past data. Environ. Res. Lett. 8.

Brammer, H., 2014. Bangladesh's dynamic coastal regions and sea-level rise. Clim. Risk Manage. 1, 51–62.

Brown, S., Nicholls, R.J., Lázár, A.N., Hornby, D.D., Hill, C., Hazra, S., Appeaning Addo, K., Haque, A., Caesar, J., Tompkins, E.L., 2018. What are the implications of sea-level rise for a 1.5, 2 and 3 °C rise in global mean temperatures in the Ganges-Brahmaputra-Meghna and other vulnerable deltas? Reg. Environ. Change 18, 1829–1842.

Caglar, B., Becek, K., Mekik, C., Ozendi, M., 2018. On the vertical accuracy of the ALOS world 3D–30m digital elevation model. Remote Sens. Lett. 9, 607–615.

Caldwell, P., Merrifield, M., Thompson, P., 2015. Sea Level Measured by Tide Gauges from Global Oceans. NOAA National Centers for Environmental Information datasets. Retrieved from http://uhslc.soest.hawaii.edu/data/?rq#uh136a.

CCC, 2016. Assessment of Sea Level Rise on Bangladesh Coast through Trend Analysis. Climate Change Cell, Department of Environment, Ministry of Environment and Forests, Dhaka, Bangladesh.

Chao, B.F., Wu, Y., Li, Y., 2008. Impact of artificial reservoir water impoundment on global sea level. Science 320, 212–214.

Cho, J., Cho, W., Jung, I., 2018. rSQM: Statistical Downscaling Toolkit for Climate Change Scenario Using Non Parametric Quantile Mapping. R package version 1.3.14. Retrieved from https://rdrr.io/cran/rSQM.

Eckstein, D., Hutfils, M.-L., Winges, M., 2019. Global Climate Risk Index. Germanwatch, Bonn.

Florinsky, I.V., Skrypitsyna, T.N., Luschikova, O.S., 2018. Comparative accuracy of the AW3D30 DSM, ASTER GDEM, and SRTM1 DEM: a case study on the Zaoksky testing ground, Central European Russia. Remote Sens. Lett. 9, 706–714.

Forsberg, R., Sørensen, L., Simonsen, S., 2017. Greenland and Antarctica ice sheet mass changes and effects on global sea level. In: Cazenave, A., Champollion, N., Paul, F., Benveniste, J. (Eds.), Integrative Study of the Mean Sea Level and Its Components. Springer International Publishing, Cham, pp. 91–106.

Gesch, D.B., 2018. Best practices for elevation-based assessments of sea-level rise and coastal flooding exposure. Front. Earth Sci. 6, 1–19.

Golyandina, N., Korobeynikov, A., 2014. Basic singular spectrum analysis and forecasting with R. Comput. Stat. Data Anal. 71, 934–954.
Golyandina, N., Korobeynikov, A., Shlemov, A., Usevich, K., 2015. Multivariate and 2D extensions of singular spectrum analysis with the Rssa package. J. Stat. Softw. 67, 1–78.
Golyandina, N., Korobeynikov, A., Zhigljavsky, A., 2018. Singular Spectrum Analysis with R. Springer-Verlag GmbH, Berlin.
Golyandina, N., Nekrutkin, V., Zhigljavsky, A.A., 2001. Analysis of Time Series Structure: SSA and Related Techniques. Chapman and Hall/CRC, London.
Grinsted, A., Moore, J.C., Jevrejeva, S., 2009. Reconstructing sea level from paleo and projected temperatures 200 to 2100 ad. Clim. Dyn. 34, 461–472.
Gudmundsson, L., Bremnes, J.B., Haugen, J.E., Engen-Skaugen, T., 2012. Technical note: downscaling RCM precipitation to the station scale using statistical transformations – a comparison of methods. Hydrol. Earth Syst. Sci. 16, 3383–3390.
Hanebuth, T.J., Kudrass, H.R., Linstädter, J., Islam, B., Zander, A.M., 2013. Rapid coastal subsidence in the central Ganges-Brahmaputra Delta (Bangladesh) since the 17th century deduced from submerged salt-producing kilns. Geology 41, 987–990.
Haque, A., Kay, S., Nicholls, R.J., 2018. Present and future fluvial, tidal and storm surge flooding in Coastal Bangladesh. In: Nicholls, R.J., Hutton, C.W., Adger, W.N., Hanson, S.E., Rahman, M.M., Salehin, M. (Eds.), Ecosystem Services for Well-Being in Deltas: Integrated Assessment for Policy Analysis. Springer International Publishing, Cham, pp. 293–314.
Haque, A., Nicholls, R.J., 2018. Floods and the Ganges-Brahmaputra-Meghna Delta. In: Nicholls, R.J., Hutton, C.W., Adger, W.N., Hanson, S.E., Rahman, M.M., Salehin, M. (Eds.), Ecosystem Services for Well-Being in Deltas: Integrated Assessment for Policy Analysis. Springer International Publishing, Cham, pp. 147–159.
Horton, B.P., Rahmstorf, S., Engelhart, S.E., Kemp, A.C., 2014. Expert assessment of sea-level rise by AD 2100 and AD 2300. Quat. Sci. Rev. 84, 1–6.
Inman, M., 2009. Where warming hits hard. Nature Reports Climate Change 3, 18–21.
IPCC, 2007. Climate change 2007: impacts, adaptation and vulnerability. In: Parry, M.L., Canziani, O.F., Palutikof, J., van der Linden, P.J., Hanson, C.E. (Eds.), Contribution of Working Group II to the Fourth Assessment Report of the Intergovernmental Panel on Climate Change. Cambridge University Press, Cambridge, UK.
IPCC, 2007b. Summary for policymakers. In: Solomon, S., Qin, D., Manning, M., Chen, Z., Marquis, M., Averyt, K.B., M.Tignor, Miller, H.L. (Eds.), Climate Change 2007: The Physical Science Basis. Contribution of Working Group I to the Fourth Assessment Report of the Intergovernmental Panel on Climate Change. Cambridge University Press, Cambridge, United Kingdom and New York, NY, USA.
IPCC, 2014. Climate change 2014: synthesis report. In: Team, Core Writing, Pachuary, R.K., Meyer, L.A. (Eds.), Contribution of Working Groups I, II and III to the Fifth Assessment Report. Intergovernmental Panel on Climate Change, Geneva.
IPCC, 2018. Summary for policymakers, in: Masson-Delmotte, V., Zhai, P., Pörtner, H.-O., Roberts, D., Skea, J., Shukla, P.R., Pirani, A., Moufouma-Okia, W., Péan, C., Pidcock, R., Connors, S., Matthews, J.B.R., Chen, Y., Zhou, X., Gomis, M.I., Lonnoy, E., Maycock, T., Tignor, M., Waterfield, T. (Eds.), Global Warming of 1.5°C: An IPCC Special Report. World Meteorological Organization, Geneva, p. 32.
Islam, M.R., 2004. Where Land Meets the Sea: A Profile of the Coastal Zone of Bangladesh. The University Press Limited, Dhaka.
JAXA, 2019. ALOS Global Digital Surface Model (DSM): ALOS World 3D-30m (AW3D30). Version 2.2. Earth Observation Research Center, Japan Aerospace Exploration Agency. Retrieved from https://www.eorc.jaxa.jp/ALOS/en/aw3d30/index.htm.
Karim, M.F., Mimura, N., 2008. Impacts of climate change and sea-level rise on cyclonic storm surge floods in Bangladesh. Global Environ. Change 18, 490–500.
Karmalkar, A., McSweeney, C., New, M., Lizcano, G., 2010. UNDP Climate Change Country Profiles: Bangladesh. Retrieved from http://www.geog.ox.ac.uk/research/climate/projects/undp-cp/UNDP_reports/Bangladesh/Bangladesh.hires.report.pdf.
Khan, A.A., 2019. Why would sea-level rise for global warming and polar ice-melt? Geosci. Front. 10, 481–494.
Korobeynikov, A., 2010. Computation- and space-efficient implementation of SSA. Statistics and Its Interface 3, 257–368.
Li, H., Sheffield, J., Wood, E.F., 2010. Bias correction of monthly precipitation and temperature fields from Intergovernmental Panel on Climate Change AR4 models using equidistant quantile matching. J. Geophys. Res. 115, 1–20.
MOEF, 2005. National Adaptation Program of Action: Final Report. Ministry of Environment and Forest, Government of Bangladesh.
Moon, T., Ahlstrøm, A., Goelzer, H., Lipscomb, W., Nowicki, S., 2018. Rising oceans guaranteed: Arctic land ice loss and sea level rise. Current Climate Change Reports 4, 211–222.
Moritz, S., Sardá, A., Bartz-Beielstein, T., Zaefferer, M., Stork, J., 2015. Comparison of Different Methods for Univariate Time Series Imputation in R. Retrieved from https://arxiv.org/abs/1510.03924.
Mörner, N.-A., 2010. Sea level changes in Bangladesh new observational facts. Energy Environ. 21, 235–249.
Mörner, N.-A., 2017. Thermal expansion. In: Finkl, C.W., Makowski, C. (Eds.), Encyclopedia of Coastal Science. Springer International Publishing, Cham, pp. 1–3.
Mörner, N.-A., 2019a. Development of ideas and new trends in modern sea level research: The pre-quaternary, quaternary, present, and future. In: Ramkumar, M., James, R.A., Menier, D., Kumaraswamy, K. (Eds.), Coastal Zone Management. Elsevier, pp. 15–62.
Mörner, N.-A., 2019b. Rotational eustasy as observed in nature. Int. J. Geosci. 10, 745–757.
Moss, R.H., Edmonds, J.A., Hibbard, K.A., Manning, M.R., Rose, S.K., Van Vuuren, D.P., Carter, T.R., Emori, S., Kainuma, M., Kram, T., 2010. The next generation of scenarios for climate change research and assessment. Nature 463, 747.
Nicholls, R.J., 2004. Coastal flooding and wetland loss in the 21st century: changes under the SRES climate and socio-economic scenarios. Global Environ. Change 14, 69–86.
Nicholls, R.J., Cazenave, A., 2010. Sea-level rise and its impact on coastal zones. Science 328, 1517–1520.
Nicholls, R.J., Hoozemans, F.M., Marchand, M., 1999. Increasing flood risk and wetland losses due to global sea-level rise: regional and global analyses. Global Environ. Change 9, S69–S87.
Nishat, A., Mukherjee, N., 2013. Sea level rise and its impacts in coastal areas of Bangladesh. In: Shaw, R., Mallick, F., Islam, A. (Eds.), Climate Change Adaptation Actions in Bangladesh. Springer, Tokyo, pp. 43–50.
Orlić, M., Pasarić, Z., 2013. Semi-empirical versus process-based sea-level projections for the twenty-first century. Nat. Clim. Change 3, 735–738.
Pethick, J., Orford, J.D., 2013. Rapid rise in effective sea-level in southwest Bangladesh: its causes and contemporary rates. Global Planet. Change 111, 237–245.
Poulter, B., Halpin, P.N., 2008. Raster modelling of coastal flooding from sea-level rise. Int. J. Geographical Information Sci. 22, 167–182.
Rahman, S., Rahman, M.A., 2015. Climate extremes and challenges to infrastructure development in coastal cities in Bangladesh. Weather Clim. Extremes 7, 96–108.
Rahmstorf, S., 2007. A semi-empirical approach to projecting future sea-level rise. Science 315, 368–370.
Rogelj, J., Meinshausen, M., Knutti, R., 2012. Global warming under old and new scenarios using IPCC climate sensitivity range estimates. Nat. Clim. Change 2, 248.
Ruane, A.C., Major, D.C., Yu, W.H., Alam, M., Hussain, S.G., Khan, A.S., Hassan, A., Hossain, B.M.T.A., Goldberg, R., Horton, R.M., Rosenzweig, C., 2013. Multi-factor impact analysis of agricultural production in Bangladesh with climate change. Global Environ. Change 23, 338–350.
Sarwar, G.M., Khan, M.H., 2007. Sea level rise: a threat to the coast of Bangladesh. Internationales Asienforum 38, 375–397.
Sarwar, M.G.M., 2013. Sea-level rise along the coast of Bangladesh. In: Shaw, R., Mallick, F., Islam, A. (Eds.), Disaster Risk Reduction Approaches in Bangladesh. Springer, Tokyo, pp. 217–231.
Singh, O.P., 2002. Spatial variation of sea level trend along the Bangladesh coast. Mar. Geod. 25, 205–212.
Tadono, T., Nagai, H., Ishida, H., Oda, F., Naito, S., Minakawa, K., Iwamoto, H., 2016. Generation of the 30 m-mesh global digital surface model by ALOS prism. International Archives of the Photogrammetry, Remote Sensing & Spatial Information Sciences 41.
UN, 2017a. Factsheet: people and oceans. The Ocean Conference, United Nations, New York, 5-9 June.
UN, 2017b. World Population Prospects. DESA/Population Division, United Nations. Retrieved from https://population.un.org/wpp/Download/Standard/Population/.
Unnikrishnan, A.S., Shankar, D., 2007. Are sea-level-rise trends along the coasts of the north Indian Ocean consistent with global estimates? Global Planet. Change 57, 301–307.
Vermeer, M., Rahmstorf, S., 2009. Global sea level linked to global temperature. Proc. Natl. Acad. Sci. 106, 21527–21532.
Wang, L., Chen, W., 2014. A CMIP5 multimodel projection of future temperature, precipitation, and climatological drought in China. Int. J. Climatol. 34, 2059–2078.